Two-dimensional imaging of the spin-orbit effective magnetic field

L. Meier* and G. Salis†
IBM Research, Zürich Research Laboratory, Säumerstrasse 4, 8803 Rüschlikon, Switzerland

E. Gini
FIRST Center for Micro- and Nanosciences, ETH Zürich, 8093 Zürich, Switzerland

I. Shorubalko and K. Ensslin
Solid State Physics Laboratory, ETH Zürich, 8093 Zürich, Switzerland

(Received 13 September 2007; revised manuscript received 9 November 2007; published 3 January 2008)

We report on spatially resolved measurements of the spin-orbit effective magnetic field in a GaAs/InGaAs quantum well. Biased gate electrodes lead to an electric-field distribution in which the quantum-well electrons move according to the local orientation and magnitude of the electric field. This motion induces Rashba and Dresselhaus effective magnetic fields. The projection of the sum of these fields onto an external magnetic field is monitored locally by measuring the electron spin-precession frequency using time-resolved Faraday rotation. A comparison with simulations shows good agreement with the experimental data.

DOI: 10.1103/PhysRevB.77.035305 PACS number(s): 78.47.−p, 71.70.Ej, 85.75.−d, 72.25.Dc

In the reference frame of a moving electron, electric fields transform into magnetic fields, which interact with the electron spin and couple it to the electron's orbital motion, leading to spin-orbit (SO) interaction. In crystals lacking an inversion center such as GaAs, effective magnetic fields due to bulk inversion asymmetry (BIA) were predicted by Dresselhaus.[1] In heterostructures, structure inversion asymmetry (SIA) leads to an effective magnetic field called the Rashba term.[2] Both contributions have been studied extensively (for a review, see Ref. 3) and are thought to play a crucial role in future spintronic devices because the coupling of the orbital and the spin degrees of freedom opens a new way to spin manipulation, for example, by flipping spins with oscillating electric fields.[4–7] The interplay between Dresselhaus and Rashba SO interactions has been studied[8,9] and proposed for use in a spin transistor.[10] For finite electron wave numbers, SO interaction leads to a spin splitting at zero external magnetic field, which is observable as a beating of Shubnikov–de Haas oscillations[11–17] and can be used to experimentally determine the strength of the total SO interaction. The zero-field spin splitting also results in a spin-selective momentum scattering and can lead to spin-dependent photocurrents,[18] which allow the determination of the ratio between the Rashba and Dresselhaus contributions by studying their directional dependence. Since SO interaction is the main reason for spin relaxation in GaAs quantum well (QW) samples, the directional dependence of spin relaxation reveals the relative strength of the Rashba and Dresselhaus terms.[19] A more direct method to get access to the SO fields is to impose a drift momentum on the conduction-band electrons by applying an in-plane electric field. This leads to two different effects: In a steady-state situation, the spins are oriented along the SO field.[20–23] If the spins of an ensemble of such drifting electrons are polarized by means of an optical pump pulse, a coherent spin precession about the SO field takes place, which has been observed using time-resolved Faraday rotation (TRFR) in a bulk GaAs epilayer.[24] Using TRFR, we have recently shown that the absolute values of both the Rashba and the Dresselhaus fields can be determined in a two-dimensional electron gas by studying the precession frequency of electron spins as a function of the electron's direction of motion with respect to the crystal lattice.[25] An oscillating electric field was applied at an arbitrary direction in the plane of an InGaAs QW using two pairs of opposed electric gates arranged perpendicularly to each other and enclosing a square area of QW electrons [see Fig. 1(a)].

Here, we study the spatial distribution of the total SO effective magnetic field between and outside the four gate electrodes that are used to generate the in-plane electric field. We show that the measured maps of spin-precession frequency can be well explained by assuming that the electrons move along the spatially varying electric field and that their spins perceive a SO effective magnetic field given by their local drift momentum. Depending on the orientation of an external magnetic field with respect to the crystal axis, the precession frequency becomes sensitive to the drift momentum component along a fixed in-plane direction, allowing one to spatially map the corresponding momentum component. A simulation with fixed values for the Rashba and Dresselhaus constants as determined in Ref. 25 leads to good agreement with the measured precession-frequency maps. Specifically, the results confirm that the electron drift momentum in the center of the gates can be described by the superposition of two perpendicular components given by the two orthogonal gate biases, as it was assumed in Ref. 25. Away from the center, however, the electric field and thus the spin-precession frequency start to vary. Large SO-induced effects on the spin-precession frequency can still be detected far away from the region between the gates because of the connection lines to the gates. This illustrates the importance of a precise definition of the electrical connection scheme in a larger setup and the difficulty of applying electric fields only at given positions of a two-dimensional electron gas.

The samples are either a 20- or 43-nm-wide InGaAs/GaAs QW as described in Ref. 25 (samples 1 and 2). We experimentally determine $B_{\mathrm{tot}}=|\boldsymbol{B}_{\mathrm{tot}}|=h\nu/g\mu_B$ by measuring the electron spin-precession frequency ν of opti-

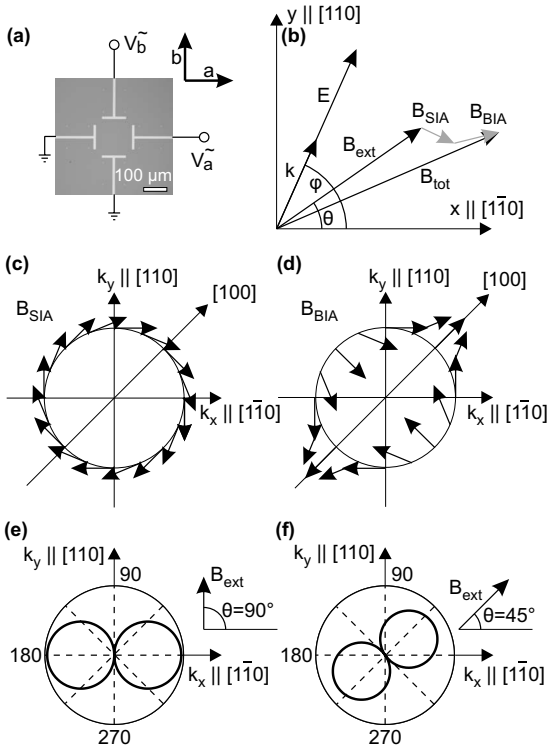

FIG. 1. (a) Microscope image of sample structure and schematic gate connections. (b) Relevant fields and angles. A magnetic field $\boldsymbol{B}_{\text{ext}}$ is applied at an angle θ with respect to the $[1\bar{1}0]$ axes and an electric field $\boldsymbol{E}$ at an angle φ. [(c) and (d)] Orientation of (c) Rashba and (d) Dresselhaus effective magnetic fields for the electron wave vector k on a unit circle. [(e) and (f)] Polar plot of $A(\theta,\varphi)$ as a function of φ for $\theta=90°$ and 45°, as calculated for $B_{\text{SIA}}=-4$ mT and $B_{\text{BIA}}=21$ mT (sample 1). Depending on θ, A is proportional to either the component of $\boldsymbol{E}_0$ perpendicular or approximately parallel to $\boldsymbol{B}_{\text{ext}}$.

cally excited conduction-band electrons using scanning TRFR (h denotes Planck's constant, g the electron g factor, and μ_B the Bohr magneton). With a first, circularly polarized pump pulse tuned to the absorption edge of the QW ($\lambda=870$ nm, average power of 400 μW, pulse width of 2 ps, and repetition rate of 80 MHz), we create a spin polarization in the QW conduction band perpendicular to the QW plane. A pump-probe delay time $\Delta\tau$ later, we probe the spin polarization with a linearly polarized probe pulse (average power of 60 μW) and monitor the rotation angle θ_F of its polarization plane. This Faraday rotation angle can be fitted to $\theta_F=\theta_0\exp(-\Delta\tau/T_2^*)\cos(2\pi\nu\Delta\tau)$ to yield both the spin-precession frequency ν and the spin-coherence time T_2^*. By spatially moving the sample relative to the laser beams, the spin dynamics can be studied with a spatial resolution limited by the diameter of the beam in the focus, here approximately 15 μm. Scanning Kerr microscopy has been used in Refs. 26 for spatially resolving nuclear imprinting effects and in Refs. 27 and 28 for studying spin transport in GaAs epilayers.

On top of the sample, four gates and the corresponding connection lines were defined using standard electron-beam lithography, evaporation of a 10-nm-thick Ti adhesion layer and a 80-nm-thick Au layer, and lift-off techniques. As shown in Fig. 1(a), opposite gate pairs were connected to phase-locked oscillators, one each for the two perpendicular directions a and b. Two neighboring gates were grounded, and by adjusting the voltage amplitudes V_a and V_b on the other two gates, an oscillating electric field $\boldsymbol{E}(t)=\boldsymbol{E}_0\sin(2\pi ft)$, $f=160$ MHz, is induced in the QW plane. In the center of the four electrodes, $\boldsymbol{E}_0$ points at an angle, with respect to the a axis, given by $\arctan V_b/V_a$. We have fabricated different samples in which the a axis is oriented along either $[1\bar{1}0]$ or $[100]$ of the semiconductor crystal. We define a coordinate system with $x\|[1\bar{1}0]$ and $y\|[110]$, and label the angle of $\boldsymbol{E}_0$ with the x axis as φ [see Fig. 1(b)]. As long as $1/f$ is large compared to the mean collision time of the electrons in the QW ($\approx$1 ps), the electrons adiabatically follow $\boldsymbol{E}(t)$ and their drift wave vector is given by $\boldsymbol{k}=m^*\mu\boldsymbol{E}(t)/\hbar$, with m^* the effective electron mass and μ the electron mobility. Furthermore, the small collision time prevents the electrons from leaving the laser focus during the time $1/f$. Because of their nonvanishing k vector, the electrons are subject to SO effective magnetic fields, which in two-dimensional systems are given by[3,29]

$$\boldsymbol{B}_{\text{SIA}}=\frac{2\alpha}{g\mu_B}\begin{pmatrix}k_y\\-k_x\end{pmatrix}\quad\text{and}\quad\boldsymbol{B}_{\text{BIA}}=\frac{2\beta}{g\mu_B}\begin{pmatrix}k_y\\k_x\end{pmatrix},\tag{1}$$

with $\boldsymbol{k}=(k_x,k_y)$ and α and β the Rashba and Dresselhaus coupling constants, respectively. The geometrical dependence on $\boldsymbol{k}$ is shown in Figs. 1(c) and 1(d). Whereas $\boldsymbol{B}_{\text{SIA}}$ is always perpendicular to $\boldsymbol{k}$, $\boldsymbol{B}_{\text{BIA}}$ points along $\pm\boldsymbol{k}$ for the $[100]$ and $[010]$ directions. When analyzing the spin precession, both SO contributions can be added to an external magnetic field $\boldsymbol{B}_{\text{ext}}$,[30,31] which we apply in the plane of the QW and at an angle θ with the x axis, as illustrated in Fig. 1(b). For all data presented, we choose $B_{\text{ext}}=0.958$ T.

If B_{SIA}, $B_{\text{BIA}}\ll B_{\text{ext}}$, the total magnetic field B_{tot} can be expressed by[25]

$$B_{\text{tot}}(t)\approx B_{\text{ext}}+A(\theta,\varphi)\sin(2\pi ft).\tag{2}$$

Here, t is the time delay between the electric-field oscillation and the pump pulse (known up to an offset t_0, which is constant in all experiments), and

$$A(\theta,\varphi)=(B_{\text{BIA}}+B_{\text{SIA}})\cos\theta\sin\varphi+(B_{\text{BIA}}-B_{\text{SIA}})\sin\theta\cos\varphi.\tag{3}$$

By probing ν at different times t, we find $B_{\text{tot}}(t)$ to oscillate with t with the frequency f. Figure 2(a) shows TRFR scans for two different t. The data are obtained on sample 1 in the center of the four gates that are aligned with the x and y axes. With $V_a=V_b=1$ V, the electric field is oriented along $[100]$ at the position of the laser focus. B_{ext} is applied along $[110]$ ($\theta=90°$). The TRFR signal monitors the coherent precession of the QW electron spins about the total field $B_{\text{tot}}(t)$. Spins precess faster for $t=-1.4$ ns than for $t=1.7$ ns. This variation of the precession frequency follows the oscillation of $\boldsymbol{E}(t)$, as becomes evident when plotting the fitted spin precession frequency ν as a function of t [see symbols in Fig. 2(b)]. The data points fit to a sinusoidal oscillation at frequency $f=160$ MHz (solid line). Except from a much weaker

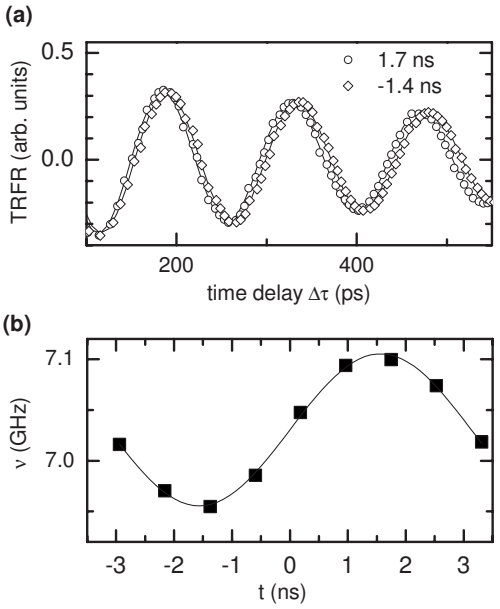

FIG. 2. (a) Measured TRFR vs $\Delta\tau$ on sample 1 with an electric field oscillating at 160 MHz along the [100] axis, and $\theta=90°$. Two curves are shown for two different times t at which the electric field has opposite signs (open symbols). The solid lines are a fit to an exponentially decaying oscillation. In (b), the obtained precession frequency ν is plotted vs t (symbols). The solid line represents a fitted harmonic oscillation at 160 MHz, yielding the amplitude $A(\theta,\varphi)$.

contribution at $2f$,[25] we do not observe higher harmonics in $\nu(t)$, from which we conclude that the linear dependence of the effective spin-orbit magnetic field on k in Eq. (1) is valid. Specifically, the terms cubic in k can be neglected. Such terms can be significant for the zero-field SO splitting[32] at the Fermi wave vector. In our case, however, the effective SO magnetic field is determined by the in-plane drift wave vector k, which is much smaller than the quantized wave number perpendicular to the QW, and therefore neglectable cubic contributions are expected.

The obtained $\nu(t)$ can be converted into $B_{\mathrm{tot}}(t)$, the amplitude of its oscillation being given by $A(\theta,\varphi)$ according to Eq. (2). By measuring $A(\theta,\varphi)$ at varying θ and φ in the center of the four gates and comparing to Eq. (3), we determine $B_{\mathrm{SIA}}=-4.2$ mT and $B_{\mathrm{BIA}}=21.6$ mT for sample 1 and $B_{\mathrm{SIA}}=-8.5$ mT and $B_{\mathrm{BIA}}=21.1$ mT for sample 2. These values were obtained for a gate-modulation amplitude of 2 V, corresponding to $E_0=2900$ V/m.[25]

In a geometrical interpretation, $A(\theta,\varphi)$ is the projection of $\boldsymbol{B}_{\mathrm{SIA}}+\boldsymbol{B}_{\mathrm{BIA}}$ onto $\boldsymbol{B}_{\mathrm{ext}}$. Because the SO fields depend linearly on E_0, $A(\theta,\varphi)$ is proportional to the projection of the local field $\boldsymbol{E}_0$ onto an axis defined by $(x,y)=[(B_{\mathrm{BIA}}-B_{\mathrm{SIA}})\sin\theta,(B_{\mathrm{BIA}}+B_{\mathrm{SIA}})\cos\theta]$. At constant θ, a spatial map of $A(\theta,\varphi)$ therefore directly images one component of $\boldsymbol{E}_0$. Figures 1(e) and 1(f) show the calculated $A(\theta,\varphi)$ using the measured values for B_{BIA} and B_{SIA} as a function of φ for $\theta=90°$ and 45° for sample 1. In the first case, A is proportional to the projection of E onto the x axis, with an amplitude of $B_{\mathrm{BIA}}-B_{\mathrm{SIA}}$. For $\theta=45°$, the projection is onto $\varphi\approx 34°$. For vanishing SIA, the highest visibility would be exactly at $\varphi=45°$.

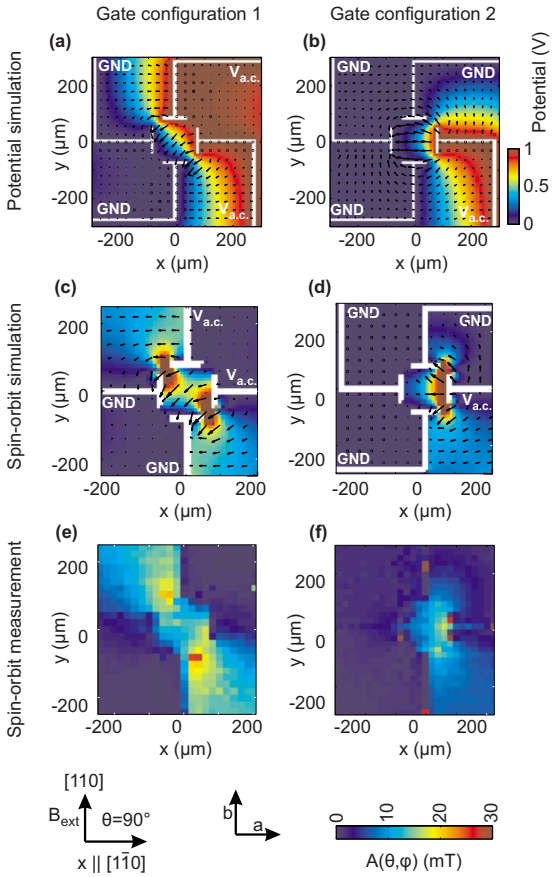

FIG. 3. (Color online) [(a) and (b)] Simulations of the electric potential (color scale) and the electric field (arrows) for two different gate potential configurations. [(c) and (d)] Simulated effective SO field and electric field (arrows). [(e) and (f)] Measured effective SO field on sample 1.

The electric field $\mathbf{E}$ is given by a superposition of the electric fields induced by the two pairs of electrodes along the a and b axis, and can be numerically determined with a partial differential-equation solver (e.g., pdetool in MATLAB) with boundary conditions given by the voltages applied to the gate electrodes and their connection lines. Figure 3 shows a situation for sample 1 with the gate electrodes oriented along the x and y axes, and at two different bias configurations, where either the top and the right gate electrode [Fig. 3(a)] or only the right gate electrode [Fig. 3(b)] was set to $V_0=1$ V, and all other gates were grounded. In the center of the electrodes, $\boldsymbol{E}_0$ points along the $[\bar{1}00]$ axis ($\varphi=225°$) or the $[\bar{1}10]$ axis ($\varphi=180°$), respectively, as expected from simply superposing two uniform fields along the x and y axes that are proportional to the two gate biases.

At every point in the two-dimensional sample plane, the local electric field gives rise to a local k vector, which allows the calculation of $A(\theta,\varphi)$ using Eqs. (1) and (3). The result of this simulation is shown in Figs. 3(c) and 3(d). Considerable SO fields are also expected away from the four gate electrodes because of the electric fields induced by the connection lines. The corresponding measurements are shown in Figs. 3(e) and 3(f). The agreement with the simulation is

good, except for the values of A measured close to a gate edge that are a factor of ≈ 2 lower than in the simulation. There, the simulation assumes perfect edges, leading to very high electric fields. In reality, the edges are rough and round, and the electric field is lower. Moreover, the simulations neglect the fact that the gates are vertically offset from the QW by 30 nm, which compared to their lateral separation of 150 μm is, however, a negligible distance.

As expected from Fig. 1(e), electric fields along x lead to high SO contributions to ν. In Figs. 3(c) and 3(e), the connection lines along y induce strong electric fields along x in the upper left and the lower right quadrants of the sample. These fields lead to a k vector in the x direction and, as visible from Fig. 1(e), to a high A. In contrast, close to the horizontal connection lines along x, the high electric fields in the y direction do not lead to visible SO fields, as in this situation, $\boldsymbol{B}_{\mathrm{SO}}$ is perpendicular to $\boldsymbol{B}_{\mathrm{ext}}$ and therefore $A=0$.

For the situation with three grounded gates [Fig. 3(f)], outside of the four gates the electric field component along x is large in the full lower right corner and partially in the upper right corner, leading to a high value of A at these positions. Inside the gates, $\boldsymbol{E}_0$ is mainly aligned along $-x$ and decays from right to left because of the shielding from the upper and lower gates which are at ground potential, which is directly observable in the measured and simulated maps of A.

In Fig. 4, we focus on the area between the four gate electrodes. We choose a configuration in which the gates and therefore the (a,b) axis are oriented at 45° to the (x,y) axis. The measurements were taken on sample 2, and for the simulations, the obtained values for B_{BIA} and B_{SIA} are used. We set $\theta=45°$, such that A is sensitive to the component of $\boldsymbol{E}_0$ approximately along $\boldsymbol{B}_{\mathrm{ext}}$, i.e., along the [100] axis [see Fig. 1(f)]. The angle φ_0 of the electric field in the center of the electrodes has been rotated by 30° in each step by varying the amplitudes $V_a=-V_0\cos(45°+\varphi_0)$ and $V_b=-V_0\sin(45°+\varphi_0)$ of the two phase-locked oscillators, connected to the bottom and the right gate electrode, respectively, with $V_0=1$ V. This direction is indicated by an arrow between the measurement (left column) and the simulation (right column). The simulation is again in good agreement with the measurement, except close to edges, where the simulated electric field and therefore also the SO fields are higher than observed.

In this configuration, A is sensitive to the horizontal component of $\boldsymbol{E}_0$, and therefore, the highest A are measured close to the right gate electrode (connected to V_b), provided that V_b is large enough. There, A is positive for $\varphi=225°$ and 195° (positive V_b) and negative for $\varphi=105°$ and 75° (negative V_b). As can be seen from the simulations in the right column of Fig. 3, the sign of A correlates with the component of $\boldsymbol{E}_0$ along [100]. For $\varphi=135°$, the left and right electrodes are grounded, and $\boldsymbol{E}_0$ points along the vertical direction in the center of the gates. On both the left and the right sides of the center, $\boldsymbol{E}_0$ turns sideways toward the respective grounded lateral electrode, leading to positive and negative values for A on the two sides. Even though the bottom electrode induces strong electric fields, only a small A is observed close to the electrode, since the field is mainly oriented along [010], i.e., perpendicular to [100]. For $\varphi=165°$, $\boldsymbol{E}_0$ has both positive and negative components along [100] close to the right gates, therefore leading to the appearance of both signs of A, as can be seen both in the simulation and in the measurement. In the corners of the square defined by the four gate electrodes, high A are measured as long as the two

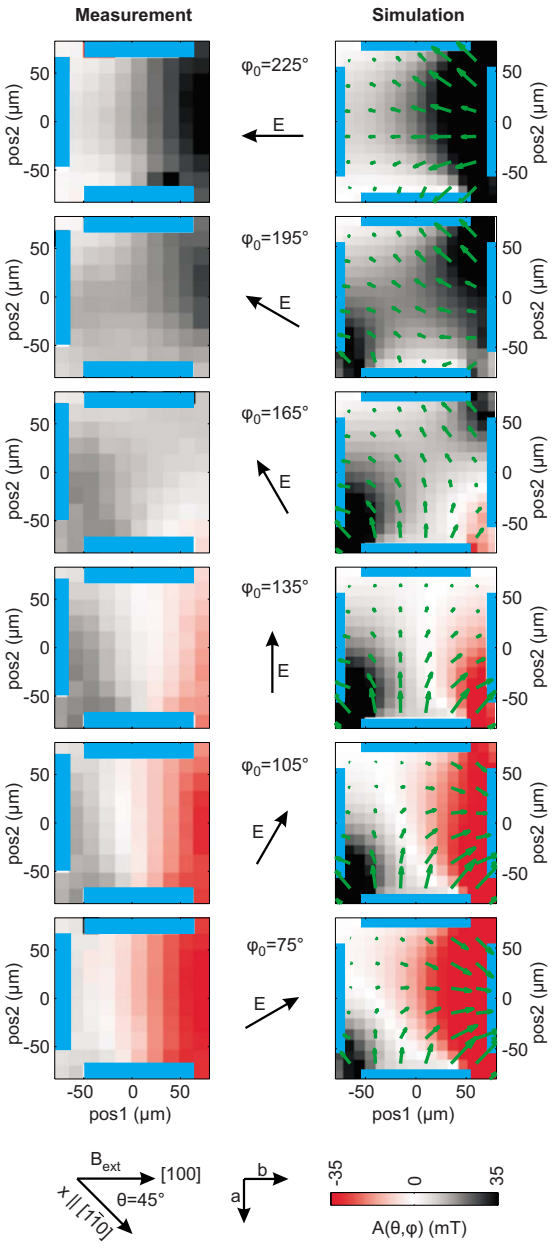

FIG. 4. (Color online) Measurement (left column) and simulation (right column) of the SO effective magnetic field between the four central gate electrodes (blue) for sample 2. The left and the upper gate electrode are grounded, and biases V_a and V_b are applied to the bottom and right electrode, respectively. The direction of the electric field in the center of the gate electrodes is indicated by black arrows. The calculated electric field is visualized as green arrows (right column). The magnetic field is applied along the [100] axis, which points to the right in the figure. In the left column, blue is used for positions where no TRFR signal could be observed because the beams were blocked by the gate electrode. The color code is different from that in Fig. 3 to visualize the sign of A.

neighboring electrodes are on different potentials. There, the electric field is diagonal and therefore has substantial components along [100].

In conclusion, we have shown that the electric field induced by biased gate electrodes modifies the electron spin precession in an InGaAs QW through the presence of a SO effective magnetic field. Spatially resolved optical measurements of the spin precession frequency are in good agreement with numerically obtained spatial maps. They confirm that the change in spin precession frequency is a measure of the projection of the drift momentum and thus the electric field along an in-plane direction that is given by the Rashba and Dresselhaus constants as well as the direction of $\boldsymbol{B}_{\mathrm{ext}}$. By adjusting the angle of $\boldsymbol{B}_{\mathrm{ext}}$, different components of the electric field can be spatially mapped. Alternatively, if the electric field is known, this technique might allow one to measure spatial variations of the Rashba and Dresselhaus constants.[33,34]

We acknowledge R. Allenspach, M. Duckheim, T. Ihn, R. Leturcq, D. Loss, and M. Witzig for helpful discussions. This work was supported by the Swiss National Science Foundation (NCCR Nanoscale Science).

*Also at Solid State Physics Laboratory, ETH Zürich, 8093 Zürich, Switzerland.
†gsa@zurich.ibm.com

[1] G. Dresselhaus, Phys. Rev. **100**, 580 (1955).
[2] Y. A. Bychkov and E. I. Rashba, J. Phys. C **17**, 6039 (1984).
[3] R. Winkler, *Spin-Orbit Coupling Effects in Two-Dimensional Electron and Hole Systems*, Springer Tracts in Modern Physics Vol. 191 (Springer, Berlin, 2003).
[4] E. I. Rashba and A. L. Efros, Phys. Rev. Lett. **91**, 126405 (2003).
[5] E. I. Rashba and A. L. Efros, Appl. Phys. Lett. **83**, 5295 (2003).
[6] M. Duckheim and D. Loss, Nat. Phys. **2**, 195 (2006).
[7] V. N. Golovach, M. Borhani, and D. Loss, Phys. Rev. B **74**, 165319 (2006).
[8] M. Duckheim and D. Loss, Phys. Rev. B **75**, 201305(R) (2007).
[9] B. A. Bernevig, J. Orenstein, and S.-C. Zhang, Phys. Rev. Lett. **97**, 236601 (2006).
[10] J. Schliemann, J. C. Egues, and D. Loss, Phys. Rev. Lett. **90**, 146801 (2003).
[11] B. Das, D. C. Miller, S. Datta, R. Reifenberger, W. P. Hong, P. K. Bhattacharya, J. Singh, and M. Jaffe, Phys. Rev. B **39**, 1411 (1989).
[12] J. Luo, H. Munekata, F. F. Fang, and P. J. Stiles, Phys. Rev. B **41**, 7685 (1990).
[13] G. Engels, J. Lange, T. Schäpers, and H. Lüth, Phys. Rev. B **55**, R1958 (1997).
[14] T. Schapers, G. Engels, J. Lange, T. Klocke, M. Hollfelder, and H. Luth, J. Appl. Phys. **83**, 4324 (1998).
[15] C.-M. Hu, J. Nitta, T. Akazaki, H. Takayanagai, J. Osaka, P. Pfeffer, and W. Zawadzki, Phys. Rev. B **60**, 7736 (1999).
[16] P. Pfeffer and W. Zawadzki, Phys. Rev. B **59**, R5312 (1999).
[17] S. Brosig, K. Ensslin, R. J. Warburton, C. Nguyen, B. Brar, M. Thomas, and H. Kroemer, Phys. Rev. B **60**, R13989 (1999).
[18] S. D. Ganichev, V. V. Bel'kov, L. E. Golub, E. L. Ivchenko, P. Schneider, S. Giglberger, J. Eroms, J. De Boeck, G. Borghs, W. Wegscheider, D. Weiss, and W. Prettl, Phys. Rev. Lett. **92**, 256601 (2004).
[19] N. S. Averkiev, L. E. Golub, A. S. Gurevich, V. P. Evtikhiev, V. P. Kochereshko, A. V. Platonov, A. S. Shkolnik, and Y. P. Efimov, Phys. Rev. B **74**, 033305 (2006).
[20] V. M. Edelstein, Solid State Commun. **73**, 233 (1990).
[21] A. G. Aronov, Y. B. Lyanda-Geller, and G. E. Pikus, Sov. Phys. JETP **73**, 537 (1991).
[22] Y. K. Kato, R. C. Myers, A. C. Gossard, and D. D. Awschalom, Phys. Rev. Lett. **93**, 176601 (2004).
[23] A. Y. Silov, P. A. Blajnov, J. H. Wolter, R. Hey, K. H. Ploog, and N. S. Averkiev, Appl. Phys. Lett. **85**, 5929 (2004).
[24] Y. Kato, R. C. Myers, A. C. Gossard, and D. D. Awschalom, Nature (London) **427**, 50 (2004).
[25] L. Meier, G. Salis, I. Shorubalko, E. Gini, S. Schön, and K. Ensslin, Nat. Phys. **3**, 650 (2007).
[26] J. Stephens, R. K. Kawakami, J. Berezovsky, M. Hanson, D. P. Shepherd, A. C. Gossard, and D. D. Awschalom, Phys. Rev. B **68**, 041307(R) (2003).
[27] S. A. Crooker and D. L. Smith, Phys. Rev. Lett. **94**, 236601 (2005).
[28] S. A. Crooker, M. Furis, X. Lou, C. Adelmann, D. L. Smith, C. J. Palmstrøm, and P. A. Crowell, Science **309**, 2191 (2005).
[29] S. Ganichev and W. Prettl, J. Phys.: Condens. Matter **15**, R935 (2003).
[30] H.-A. Engel, E. I. Rashba, and B. I. Halperin, Phys. Rev. Lett. **98**, 036602 (2007).
[31] V. Kalevich and V. Korenev, JETP Lett. **52**, 230 (1990).
[32] J. B. Miller, D. M. Zumbühl, C. M. Marcus, Y. B. Lyanda-Geller, D. Goldhaber-Gordon, K. Campman, and A. C. Gossard, Phys. Rev. Lett. **90**, 076807 (2003).
[33] E. Y. Sherman, Appl. Phys. Lett. **82**, 209 (2003).
[34] M.-H. Liu and C.-R. Chang, Phys. Rev. B **74**, 195314 (2006).